Article DOI- https://doi.org/10.1016/j.applthermaleng.2023.121655

Accepted Manuscript

Impact of Parasitic Heat Fluxes on Deep Sub-ambient Radiative Coolers under variable Pressure © 2023 by Udayan Banik, Hosni Meddeb, Dennis Berends, Nies Reininghaus, Oleg Sergeev, Luisa Busch, Kai Gehrke, Martin Vehse, Carsten Agert is licensed under CC BY-NC-ND 4.0. To view a copy of this license, visit http://creativecommons.org/licenses/by-nc-nd/4.0/

Supplementary Section- Impact of Parasitic Heat Fluxes on Deep Sub-ambient Radiative Coolers under variable Pressure

Udayan Banik, Hosni Meddeb, Dennis Berends, Nies Reininghaus, Oleg Sergeev, Luisa Busch, Kai Gehrke, Martin Vehse, Carsten Agert*

German Aerospace Center, DLR Institute of Networked Energy Systems, 26129, Oldenburg, Germany

** Corresponding author*

Manuscript

1 ANGULAR EMISSIVITY AND THICKNESS OF SAMPLE

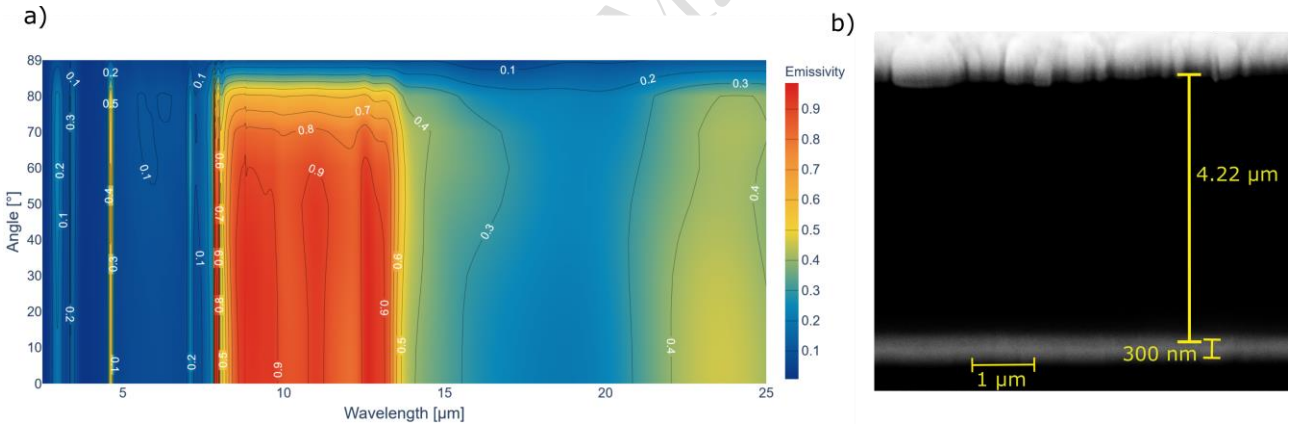

Supplementary Figure S1. a) Angular dependence of emissivity of the RSC structure. b) SEM cross section of the image

2 SPECTRAL RESPONSE OF ZNSE CONVECTIVE SHIELD

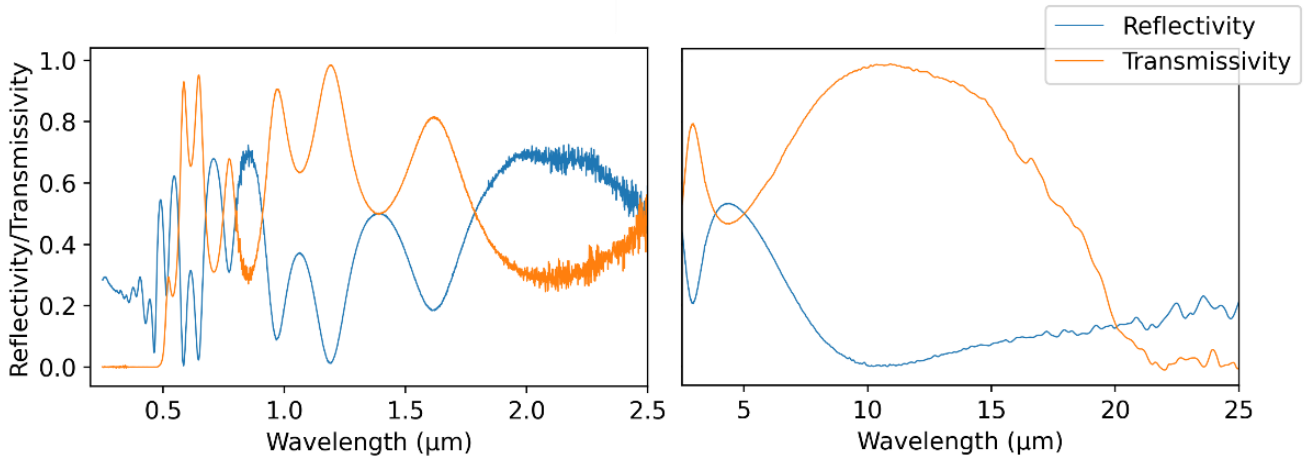

Supplementary Figure S2. Reflectivity and Transmissivity of the ZnSe cover window in between 0.3 – 2.5 μm and 2.5 -25 μm

The impact of the ZnSe window was taken into consideration using equations that were simplified and adapted from [1,2]. The below transfer function equation was used for the adapted emissivity of the RSC $\varepsilon'_{emitter}$:

$$\varepsilon'_{emitter}(\lambda,\theta)=\varepsilon_{emitter}(\lambda,\theta)\times\frac{\tau_{window}(\lambda,\theta)+\alpha_{window}(\lambda,\theta)}{1+\varrho_{window}(\lambda,\theta)\times(\varepsilon_{emitter}(\lambda,\theta)-1)} \quad \text{Eq. S1}$$

where $\varepsilon_{emitter}$ is the emissivity of the RSC at wavelength λ and angle θ and τ_{window}, α_{window}, ϱ_{window} is the transmissivity, absorptivity and reflectivity of the ZnSe window respectively. For simplicity, it was assumed that the emissivity of the ZnSe does not change with angle. Since the ZnSe window and the cone also have an impact on the incoming radiation incident on the sample, the adapted emissivity of atmosphere (ε'_{atms}) is described as below:

$$\varepsilon'_{atms}(\lambda,\theta)=\frac{[\varepsilon_{atms}(\lambda,\theta_{escape})\times R_{conc}\times\tau_{window}(\lambda,\theta)]+\alpha_{window}(\lambda,\theta)+\tau_{window}(\lambda,\theta)[1-R_{conc}]}{1+\varrho_{window}(\lambda,\theta)\times(\varepsilon_{emitter}(\lambda,\theta)-1)} \quad \text{Eq. S2}$$

where ε_{atms} is the emissivity of the atmosphere at wavelength λ and angle θ, R_{conc} is total reflectivity of a photon after sequential reflections with the cone assumed from literature to be 0.80, θ_{escape} is the direction of the photon escaping after sequential reflections assumed to be at 0° for our indoor setup with a thin atmosphere and an adjacent thermal sink of LN.

Accepted Manuscript

3 EXPERIMENTAL & MODELING CONSIDERATIONS

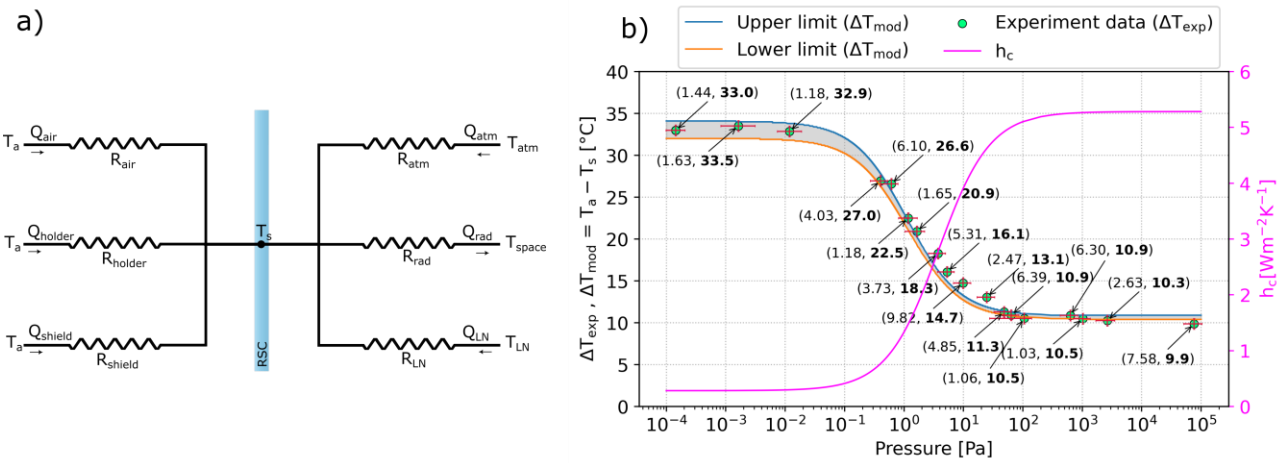

Supplementary Figure S3 a) Thermal resistance network diagram to demonstrate the heat flow in and out of the RSC, b) experimental temperature difference (ΔT_{exp}) and modelled temperature difference (ΔT_{exp}) plotted as a function of varying pressure (Figure 4 in Main Manuscript). The significant digits of the pressure and temperature (in bold) are annotated for each point in parenthesis.

The parasitic thermal resistances in Supplementary Figure S3(a) are explained using the below equations:

$$R_{air} = \frac{l_{gap}}{k_{air\text{-}atm}\left(1+7.657\times10^{-5}\left(\frac{T_a}{P\times l_{gap}}\right)\right)} \quad \text{Eq. S3}$$

$$R_{holder} = \frac{l_{holder}}{r\times k_{holder}} \quad \text{Eq. S4}$$

$$R_{shield} = \frac{(N+1)(2-\varepsilon_{shield})}{4\varepsilon_{shield}\sigma T_{shield}^{3}} \quad \text{Eq. S5}$$

Comments- We found out through experimentation, that maintaining consistent set pressure points outdoors under varying temperature for extended periods of time, sufficient enough to carry out the measurements was unattainable due to uncontrollable environmental factors (solar irradiation, wind, humidity and cloud cover). These parameters largely influence the experimental apparatus along with the pumps. One could see the notable advantage in carrying out this experiment indoors. The smooth ambient

Accepted Manuscript

temperature curves and pressure with minimal variation enabled us to have controlled and reproducible measurements (Figure 3 in Main Manuscript). To remain consistent with all the indoor measurements, the dimensions of the setup were left unaltered throughout the experiment with occasional refilling of the LN container. To negate the effect of resistive heat release to the sample by the Pt100 sensor and maximize accuracy, pulsed signals were provided to the sensors at 10 second intervals for each temperature measurement.

4 IMPACT DUE TO RISE IN EFFECTIVE TEMPERATURE OF THE HEAT SINK

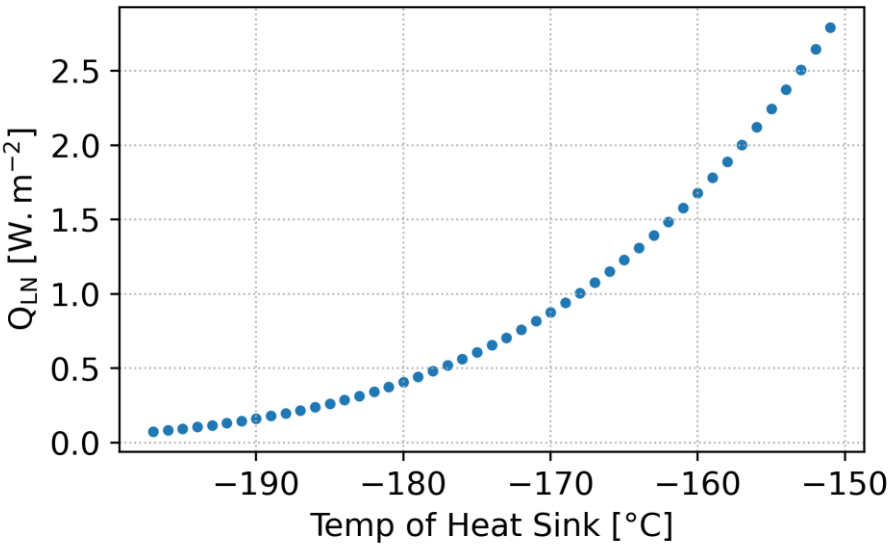

Supplementary Figure S4. Variation of the heat flux from the liquid nitrogen cryogenic sink to the sample in an ideal scenario. The rise of the effective temperature of heat sink indicates the possibility of LN partially drying up and the sample partly viewing the cold black aluminum walls instead of the LN.

5 IMPACT OF THE CONE ON RSC PERFORMANCE

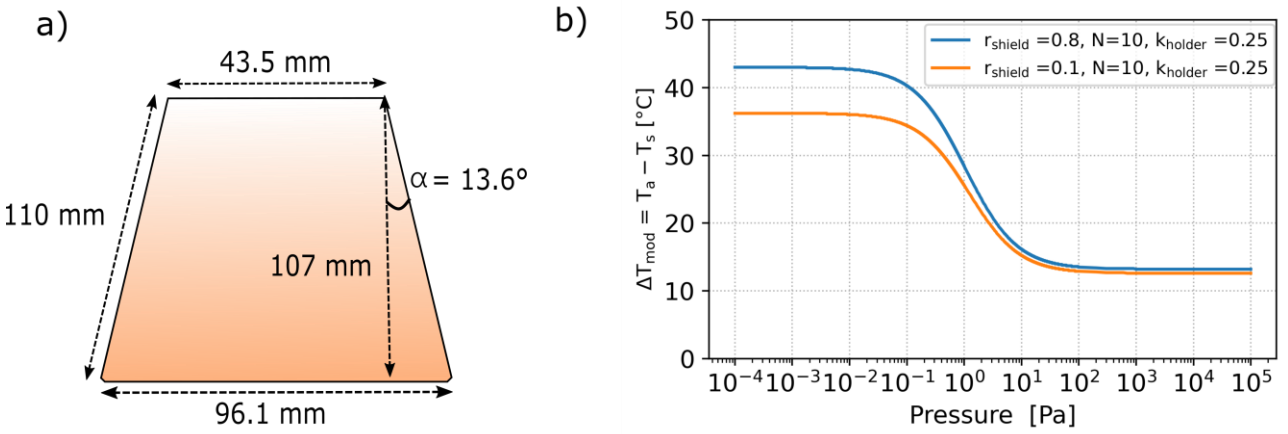

Supplementary Figure S5.a) Dimensions of the cone used for the experiment b) Equilibrium temperature for the RSC when R_{conc} factor of the cone is increased to 0.97, keeping all other parameters constant. The geometry of the cone does play a significant role on the equilibrium temperature of the RSC for this experiment as it will do for the outdoor performance.

As explained in previous studies, the cone plays a decisive role in restricting the angular view of the sky by the sample and in concentrating the outgoing radiation of the RSC to the lowest emissive part of the sky [1–3]. As described in the Materials & Methods Section 2.3.1 of the main manuscript, a silver deposited adhesive Kapton tape was used to cover the inner side of the plastic cone to make it highly reflective. The dimensions of the cone are provided in Supplementary Figure S5 (a). However, before and after measurements of the reflective tape revealed that the inner reflective surface of the cone degraded over time reducing its reflectivity. Due to the long span of the experiment for getting all the required measurement points, we decided to continue with it for the sake of simplicity and consistency. Therefore, for our indoor measurements (Figure 4) we adjusted the R_{conc} of the cone to be 0.8 (worst case scenario) while considering the geometry. Nonetheless, a better reflective cone can be easily manufactured with materials like polished Aluminum or Mylar coated sheets. The impact of a cone with a better R_c of 0.97 on the end performance is shown in Supplementary Figure S5 (b).

Accepted Manuscript

6 QUANTIFYING PARASITIC LOSSES FROM AN RSC IN VACUUM

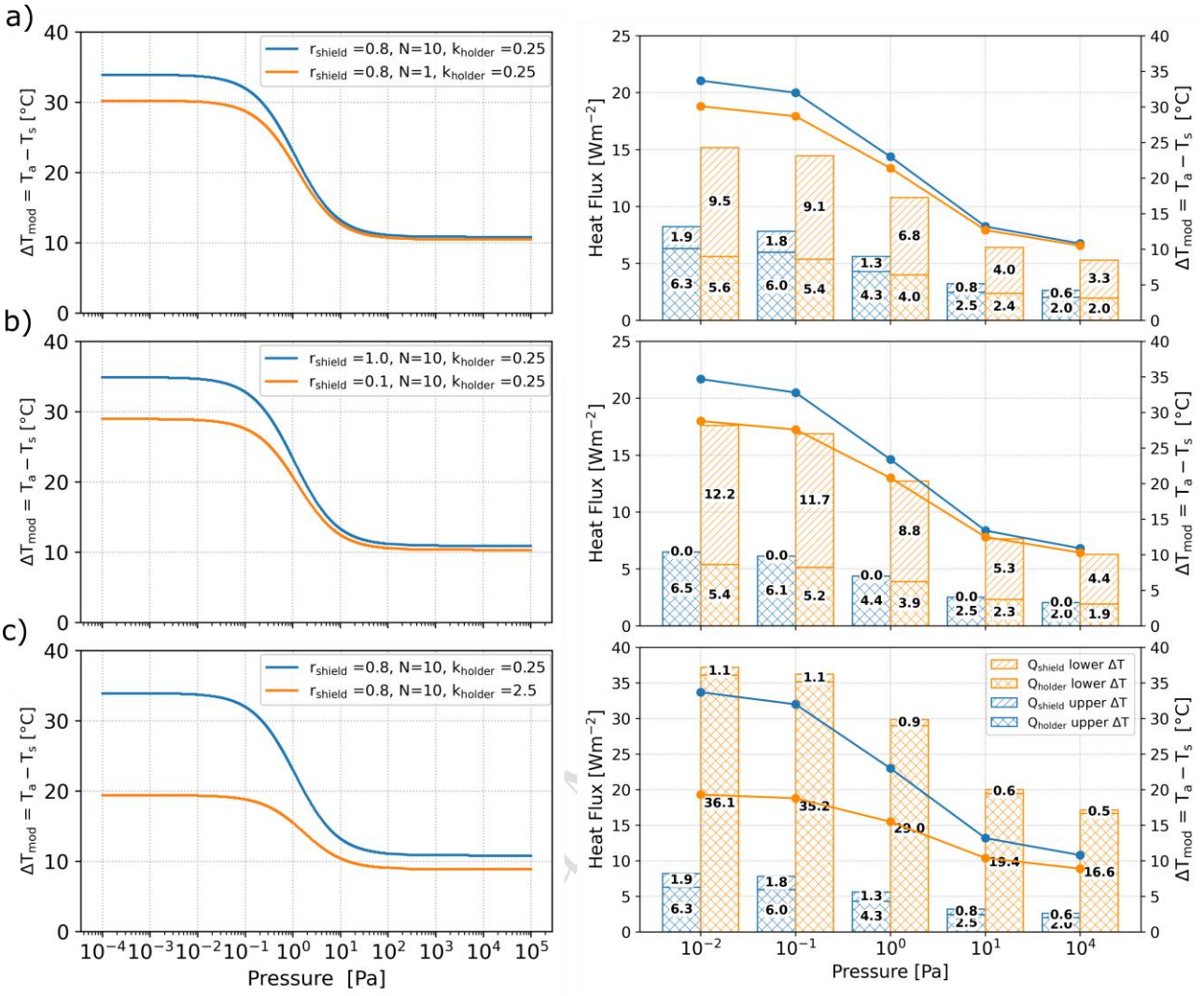

Supplementary Figure S6. Predictive behavior of an RSC as a function of pressure for similar scenarios as presented in Figure 5 in the main text. Each bar chart on the right represents the individual parasitic heat flux losses for each case. The blue and orange line with filled circle markers represents the modelled upper and lower ΔT values for each pressure value. A common legend for the bar chart is provided in figure (c)

7 BEST AND WORST CASE FOR SUBCOMPONENTS AND RATIONAL DESIGN

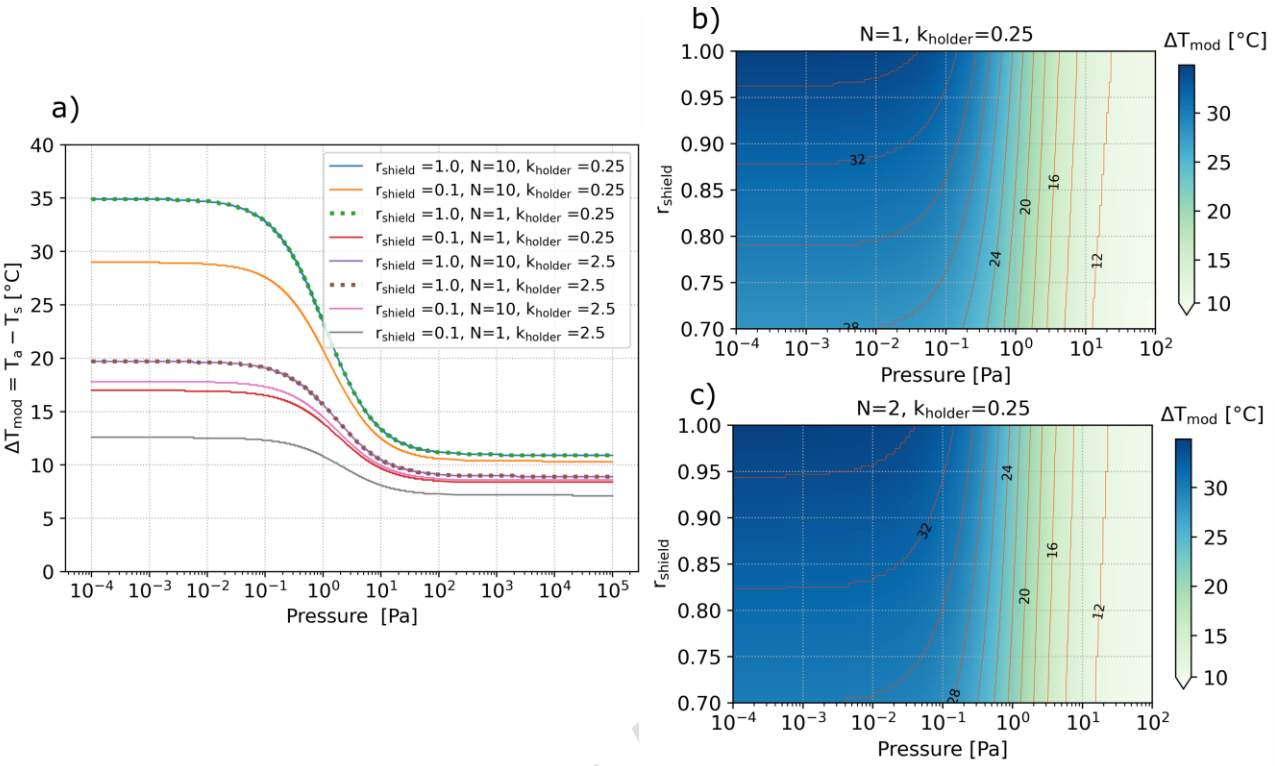

Supplementary Figure S7. a) Temperature difference fit curve at different pressures for various reflectivity of shields, number of shields and thermal conductivity of holder. R_{conc} of 0.80 was used for the analysis; temperature contour plot of the RSC in transient and low-pressure regime for r_{shield} varying between 0.7-1.0 k_{holder} = 0.25 and b) N=1 c) N=2

Accepted M

8 RADIATIVE SHIELDING EFFECT ESTIMATION

The radiative heat transfer coefficient from the shields to the RSC is represented using the below formulae Eq. S6. It is the extended representation of radiation exchange between multiple parallel planes (or shields) and radiation leaving the outer most surface, where the temperature and emissivity of the shields is assumed to be same.[4–7] It is to be noted that Eq. S7, which has been used in previous studies is a generalized version of the same formula.[1,8]

$$h_{shield} = \frac{4\varepsilon_{shield}\sigma T^3_{shield}}{(N+1)(2-\varepsilon_{shield})} \quad \text{Eq. S6}$$

$$h_{shield} = \frac{4\varepsilon_{shield}\sigma T^3_{shield}}{(2N)} \quad \text{Eq. S7}$$

Using Eq. S7 instead Eq. S6 has a nominal change on the outcome of the model's validation of the experimental results (Figure 4). This is because for our experiments the N is high and ε_{shield} is low, similar to prior studies. However, for hypothetical cases and predictive performance modelling with a smaller number of shields (N) and/or high ε_{shield}, some variation can be expected (as shown below).

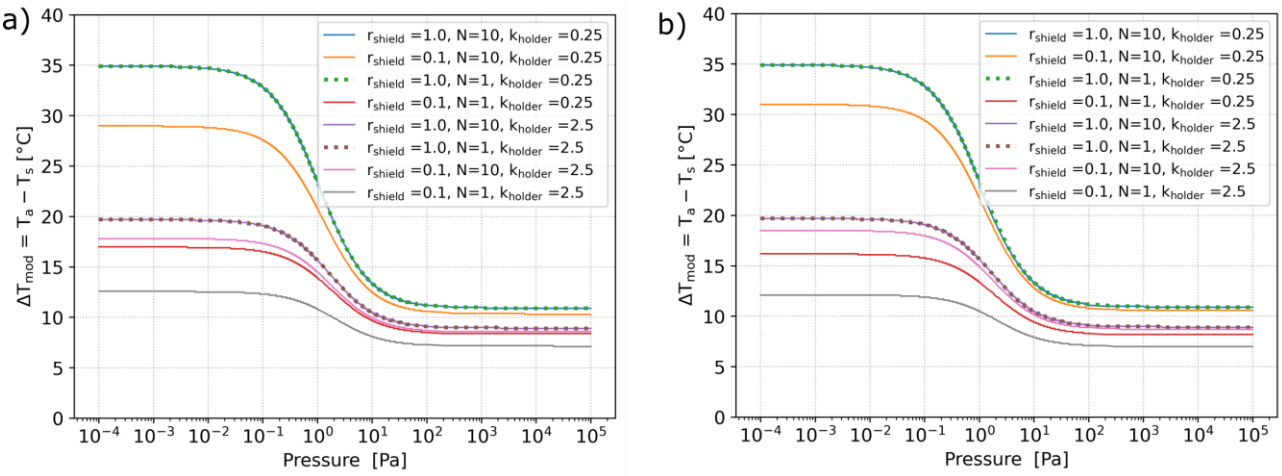

Supplementary Figure S8. Temperature difference fit curve at different pressures for various reflectivity of shields, number of shields and thermal conductivity of holder where in a) Eq. S6 was used (same as Supplementary Figure S7 (a)) and in b) Eq. S7 was used.

Accepted Manuscript

9 USE OF ARGON AS AN INSULATING MEDIUM

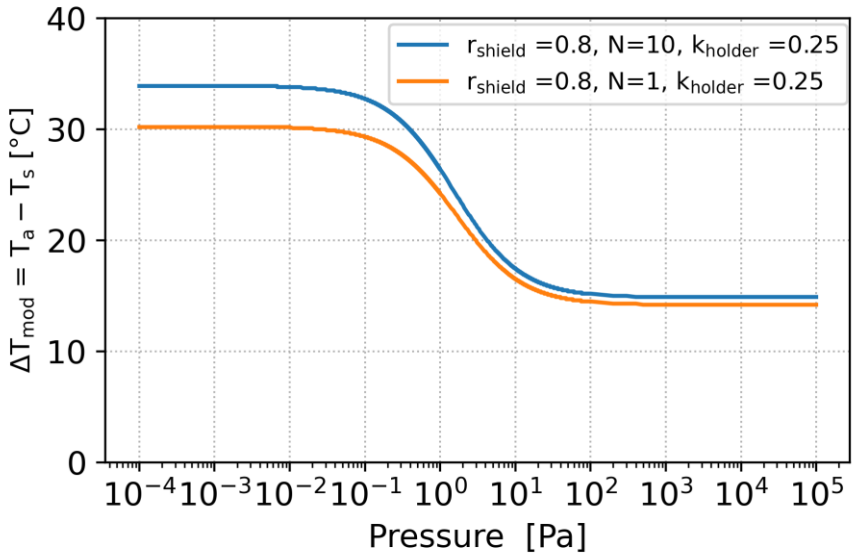

Supplementary Figure S9. Simulated performance of the RSC in Argon environment.

Due to the low thermal conductivity of Argon gas (k_{Ar} = 0.0178 $Wm^{-1}K^{-1}$) there is an immediate betterment of ΔT performance (~ 15 °C compared to 10 °C in air) at atmospheric pressure, since the conductive parasitic losses from the RSC are reduced due to the medium. Clearly, changing to a low thermally conductive gas will not bring any benefit at low-pressures regimes due to absence of the gas medium.

Accepted Manuscript

10 References

[1] Z. Chen, L. Zhu, A. Raman, S. Fan, Radiative cooling to deep sub-freezing temperatures through a 24-h day-night cycle, Nature communications, 7, (2016), 13729, 10.1038/ncomms13729.

[2] M. Dong, L. Zhu, B. Jiang, S. Fan, Z. Chen, Concentrated radiative cooling and its constraint from reciprocity, Optics express, 30, (2022), 275–285, 10.1364/OE.445544.

[3] I. Haechler, H. Park, G. Schnoering, T. Gulich, M. Rohner, A. Tripathy, A. Milionis, T.M. Schutzius, D. Poulikakos, Exploiting radiative cooling for uninterrupted 24-hour water harvesting from the atmosphere, Science advances, 7, (2021), 10.1126/sciadv.abf3978.

[4] F.P. Incropera, D. Dewitt, T. Bergman, Fundamentals of heat and mass transfer, 6th ed., John Wiley, Hoboken NJ, 2007.

[5] J. Duffie, A. Beckman, Solar Engineering of Thermal Processes, Wiley, 2013.

[6] B. Baudouy, Heat Transfer and Cooling Techniques at Low Temperature, in: Proceedings of the CAS-CERN Accelerator School: Superconductivity for Accelerators, 10.5170/CERN-2014-005.329.

[7] R.J. Howell, M.P. Menguc, R. Siegel, Thermal radiation heat transfer, CRC Press Taylor & Francis Group, Boca Raton, 2016.

[8] X. Ao, B. Li, B. Zhao, M. Hu, H. Ren, H. Yang, J. Liu, J. Cao, J. Feng, Y. Yang, Z. Qi, L. Li, C. Zou, G. Pei, Sup-Self-adaptive integration of photothermal and radiative cooling for continuous energy harvesting from the sun and outer space.

Accepted Manuscript